

Universal constrained power flow control for four-wire grid-tied power electronics converters

Citation for published version (APA):

González Duguet, C., Costa, L. F., & Papafotiou, G. (2025). Universal constrained power flow control for four-wire grid-tied power electronics converters. In *2025 IEEE Conference on Control Technology and Applications, CCTA 2025* (pp. 892-897). Article 11151467 Institute of Electrical and Electronics Engineers. <https://doi.org/10.1109/CCTA53793.2025.11151467>

DOI:

[10.1109/CCTA53793.2025.11151467](https://doi.org/10.1109/CCTA53793.2025.11151467)

Document status and date:

Published: 11/09/2025

Document Version:

Accepted manuscript including changes made at the peer-review stage

Please check the document version of this publication:

- A submitted manuscript is the version of the article upon submission and before peer-review. There can be important differences between the submitted version and the official published version of record. People interested in the research are advised to contact the author for the final version of the publication, or visit the DOI to the publisher's website.
- The final author version and the galley proof are versions of the publication after peer review.
- The final published version features the final layout of the paper including the volume, issue and page numbers.

[Link to publication](#)

General rights

Copyright and moral rights for the publications made accessible in the public portal are retained by the authors and/or other copyright owners and it is a condition of accessing publications that users recognise and abide by the legal requirements associated with these rights.

- Users may download and print one copy of any publication from the public portal for the purpose of private study or research.
- You may not further distribute the material or use it for any profit-making activity or commercial gain
- You may freely distribute the URL identifying the publication in the public portal.

If the publication is distributed under the terms of Article 25fa of the Dutch Copyright Act, indicated by the "Taverne" license above, please follow below link for the End User Agreement:

www.tue.nl/taverne

Take down policy

If you believe that this document breaches copyright please contact us at:

openaccess@tue.nl

providing details and we will investigate your claim.

Universal constrained power flow control for four-wire grid-tied power electronics converters

Cristóbal González¹, Levy Costa¹, George Papafotiou¹

Abstract—Low-voltage four-wire grids have undergone significant changes in recent decades. New power electronics-based resources have been integrated into the system, enhancing its flexibility but also impacting its stability and safety. As a result, modern control strategies must consider safety aspects and directly contribute to converter protection while supporting the network during faults. In this paper, we build upon the nonlinear model predictive control formulation proposed in [1] for three-wire systems and tackle the control design challenges and performance requirements that are present in four-wire grid-connected power electronics converters. This entails not only extending the modeling to describe the dynamics of the system's common-mode components, but also capturing the coupling of the different variable components through the control problem's constraints. The new extended formulation is tested through simulations of both symmetrical and asymmetrical faults, showing effective current and voltage limitation while performing as demanded by grid codes.

I. INTRODUCTION

Low-voltage (LV) networks have drastically changed in the last decades. From being an aggregation of passive loads to also integrating distributed generation, nonlinear loads, and energy storage, even leading to microgrids with self-sufficient capabilities. The presence of new power electronics-based actors, such as inverter-based resources (IBR) and battery energy storage systems (BESS) has led to improvements in power systems' safety and availability. These improvements arise from the power converters used to interface these IBRs and BESSs, which increase the controllability of voltage and power flow in different buses of the grid. However, these benefits come with challenges that must be addressed to prevent the integration of these new actors from becoming detrimental.

The reduction in the share of power being transferred by electrical machines, caused by the expansion of power electronics-based resources, heavily impacts system stability, as the total inertia is also reduced. Additionally, most of these resources require a phase-locked-loop (PLL) to synchronize with the grid voltage. Since LV networks are generally weak, stability issues can occur during operation at high current values or during disturbances [2]. The aforementioned stability issues, together with the limited overcurrent and overvoltage capabilities of power electronics converters, significantly affect system performance during faults. This

can lead to the forced disconnection of power electronics-based resources to prevent damage.

As a solution, grid-forming (GFM) control has shown promising results in three-wire systems. Its benefit comes from its power synchronization concept, which produces a more stable performance [3], by not requiring a PLL, and better fault-ride-through due to its voltage source behavior [4]. Since GFM converters do not directly control the converter current, many current limitation techniques have been developed to provide safe operation of the converter. However, most research focuses on balanced operation and disturbances in three-wire systems, while current limiting for unbalanced scenarios has not been widely discussed, and the four-wire case, despite its significant practical relevance, has so far remained outside the main focus of the research community [5], [6]. Moreover, during asymmetrical faults, current limitation methods tailored for balanced scenarios can lead to overcurrents in the affected phases or even overvoltages, which can be equally destructive for power semiconductors and passive components, in the unaffected ones [6]. Additionally, most strategies rely on the proper identification and separation of sequences during the fault, slowing the converter's dynamic response [6].

In practice, many single-phase loads are usually connected to LV networks, be industrial or residential ones. This means not only that the system is unbalanced but also that access to a neutral wire is needed, resulting in the circulation of common-mode currents. Hence, either a four-wire converter topology or a low-frequency transformer with connection to the neutral is needed. Some strategies have been developed for four-wire systems, but many of them require a bulky and expensive low-frequency transformer to provide current limitation [7]. For four-wire converters, overshoots immediately after fault inception can occur since constraints are not directly posed over the states of the system [8]. In addition, the requirement for the converter and its filter to behave as a balanced voltage source behind impedance has been adopted in recent grid codes such as [9], and should be achieved in both balanced and unbalanced situations.

In the previous work [1], the authors formulated a nonlinear model predictive control (MPC) strategy for three-wire grid-connected converters. The ability of MPC to deal with complex multivariable problems that involve nonlinear plants and constraints is exploited, formulating nonlinear power flow equations that result from not using PLLs for grid synchronization. This approach also allows for directly posing constraints over the system states, preventing not only overcurrents but also overvoltages on sensitive components

*This project is supported and financed by Alfen N.V. and co-financed by Holland High Tech with PPP-allowance for research and development in the HTSM top sector

¹All authors are with the Electromechanics and Power Electronics group, Department of Electrical Engineering, Eindhoven University of Technology, Eindhoven, the Netherlands

{c.a.gonzalez.duguet, l.costa, g.papafotiou}@tue.nl

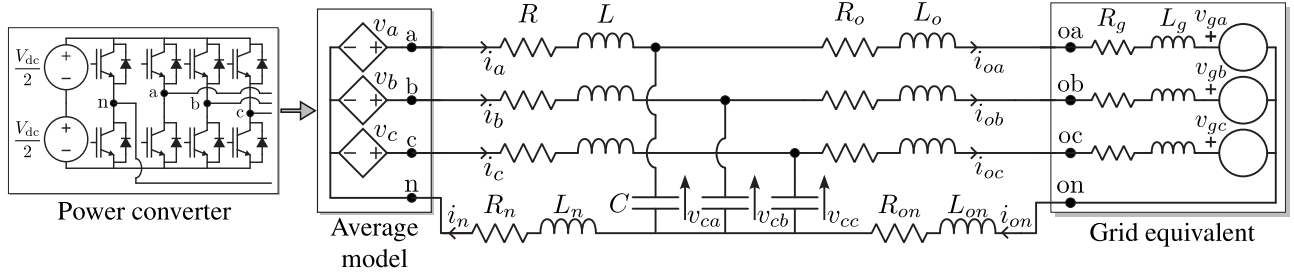


Fig. 1: Circuit diagram of a four-wire LCL filter grid-tied voltage source converter.

and guaranteeing the safe operation of the converter.

This paper extends the formulation in [1] to incorporate the common-mode variables that appear when directly connecting a four-leg converter to a four-wire system. Although the extension of the modeling of the common-mode dynamics is straightforward, as these are decoupled from the differential-mode dynamics of the system, the two different dynamic modes are coupled through the system's constraints, leading to more intricate dynamic behavior during fault scenarios and a more challenging control design task. Specifically, the contributions of the work presented here are as follows: 1) it provides constraint satisfaction during both balanced and unbalanced faults by simultaneously controlling differential- and common-mode components of a four-wire system; 2) it provides a balanced voltage source behind impedance behavior even during unbalanced faults, which is a relevant performance requirement for four-wire grid-connected converters in new grid codes such as [9], and 3) it fully utilizes the converter's capabilities by reaching the maximum allowed current during faults.

II. MODEL OF THE SYSTEM

In this section, the model of a four-wire grid-tied VSC with an LCL output filter is presented.

Consider the VSC in Fig. 1, connected to a system with nominal frequency ω_n . For control purposes, all three-phase variables, originally in the natural abc reference frame, are transformed into a $dq\gamma$ frame, where γ corresponds to the common mode part of the abc variables. The convenience of this transformation lies in the fact that dq components are independent of γ components when the passive elements of the circuit are balanced, even if the connected sources are unbalanced. Therefore, the model of dq variables is developed separately from that of γ variables. In contrast, all phases in the abc frame are coupled in such a scenario, increasing the complexity of the control problem.

A. The dq model

The modeling of dq dynamics is the same as in [1], so it is briefly presented here. First, the variables in the abc reference frame $\xi = [\xi_a \ \xi_b \ \xi_c]^\top$ are transformed into the dq quadrature rotating frame $\xi_{dq} = [\xi_d \ \xi_q]^\top$ using the standard amplitude invariant transformation (see [1]) with an angular position θ , which is defined as $\theta(t) = \omega_n t + \theta_0$, where θ_0 is an arbitrary initial angular position and ω_n is the nominal angular frequency of the grid.

The grid is modeled as a four-wire Thevenin equivalent, which means that the passive components and the voltage $v_{g,abc}$ are only representations of a more complex system. The DC link voltage is assumed to be constant and perfectly stiff. The models of system dynamics are derived by assuming an average model and not a switching model. Hence, the converter can be replaced by controlled voltage sources, as illustrated in Fig. 1.

The state-space model of the dq dynamics is written as

$$\begin{aligned} \dot{\mathbf{x}}(t) &= \mathbf{F}\mathbf{x}(t) + \mathbf{G}\mathbf{u}(t) + \mathbf{M}\mathbf{w}(t), \\ \mathbf{y}(t) &= \mathbf{f}(\mathbf{x}(t)), \end{aligned} \quad (1)$$

where the state, input, and disturbance vectors are defined as $\mathbf{x} = [i_{dq}^\top \ i_{o,dq}^\top \ v_{c,dq}^\top]^\top$, $\mathbf{u} = \mathbf{v}_{dq}$, and $\mathbf{w} = \mathbf{v}_{o,dq}$, with voltages \mathbf{v}_{abc} and $\mathbf{v}_{o,abc}$ defined with respect to their corresponding neutral points, i.e., $\mathbf{v} = [v_a - v_n, v_b - v_n, v_c - v_n]^\top$ and $\mathbf{v}_o = [v_{oa} - v_{on}, v_{ob} - v_{on}, v_{oc} - v_{on}]^\top$. The dynamic equations of the system are derived from Kirchhoff's laws, with all variables and parameters in per unit [10]. Thus, the dq matrices are

$$\begin{aligned} \mathbf{F} &= \omega_B \begin{bmatrix} -\frac{R}{L}\mathbf{I}_2 - \omega_n \mathbf{J} & \mathbf{0}_2 & -\frac{1}{L}\mathbf{I}_2 \\ \mathbf{0}_2 & -\frac{R_o}{L_o}\mathbf{I}_2 - \omega_n \mathbf{J} & \frac{1}{L_o}\mathbf{I}_2 \\ \frac{1}{C}\mathbf{I}_2 & -\frac{1}{C}\mathbf{I}_2 & -\omega_n \mathbf{J} \end{bmatrix}, \\ \mathbf{G} &= \frac{\omega_B}{L} [\mathbf{I}_2 \ \mathbf{0}_{4 \times 2}]^\top, \quad \mathbf{M} = -\frac{\omega_B}{L_o} [\mathbf{0}_2 \ \mathbf{I}_2 \ \mathbf{0}_2]^\top, \end{aligned}$$

where \mathbf{I}_n is the identity matrix of order n , $\mathbf{0}_{n \times m}$ is an n by m zero matrix, $\mathbf{0}_n$ is a square zero matrix of order n , and

$$\mathbf{J} = \begin{bmatrix} 0 & -1 \\ 1 & 0 \end{bmatrix}.$$

Regarding the output of the system, the controller must regulate the power flow at the output of the converter and follow specific references. Active and reactive power references must be tracked exclusively by dq components. That is, the average power transferred by γ components must be zero. Hence, the output $\mathbf{y}(k) = \mathbf{f}(\mathbf{x}(k)) = [pq]^\top$, are the instantaneous active and reactive power p and q defined as

$$p = v_{cd}i_d + v_{cq}i_q, \quad q = v_{cq}i_d - v_{cd}i_q. \quad (2)$$

Notice that the output definition makes the system nonlinear. However, because of this definition, it is possible to control the power flow while considering the voltage at the point of connection as a disturbance. This avoids the necessity of a phase-locked-loop to synchronize with the grid.

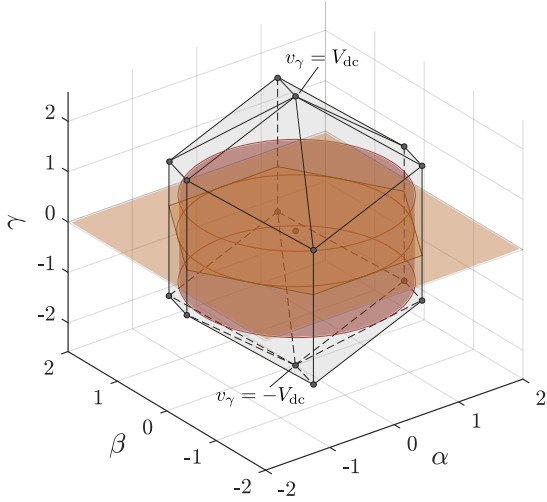


Fig. 2: Feasible set of voltages of a four-legs two-level inverter, together with the control set used for the MPC formulation.

Model (1) can be discretized with a sampling period T_s using exact discretization, resulting in

$$\begin{aligned} \mathbf{x}(k+1) &= \mathbf{A}\mathbf{x}(k) + \mathbf{B}\mathbf{u}(k) + \mathbf{T}\mathbf{w}(k), \\ \mathbf{y}(k) &= f(\mathbf{x}(k)), \end{aligned} \quad (3)$$

where the matrices are $\mathbf{A} = e^{\mathbf{F}T_s}$, $\mathbf{B} = -\mathbf{F}^{-1}(\mathbf{I}_6 - \mathbf{A})\mathbf{G}$, and $\mathbf{T} = -\mathbf{F}^{-1}(\mathbf{I}_6 - \mathbf{A})\mathbf{M}$.

B. The γ model

Because of the presence of a neutral wire, the common-mode component of all variables must be incorporated into the analysis. This component, denoted by the subindex γ , is defined as

$$\xi_\gamma = \frac{1}{3}(\xi_a + \xi_b + \xi_c), \quad (4)$$

and, for currents, it is equivalent to one third of the corresponding neutral current; that is, $i_n = 3i_\gamma$, $i_{on} = 3i_{o,\gamma}$.

The procedure for developing the γ model is the same as for the dq variables. Consider the state vector $\mathbf{x}_\gamma = [i_\gamma \ i_{o,\gamma} \ v_{c,\gamma}]^\top$, the actuation $u_\gamma = v_\gamma$, the disturbance $w_\gamma = v_{o,\gamma}$, and the matrices derived from Kirchoff's laws

$$\mathbf{F}_\gamma = \omega_B \begin{bmatrix} -\frac{R+3R_n}{L+3L_n} & 0 & -\frac{1}{L+3L_n} \\ 0 & -\frac{R_o+3R_{on}}{L+3L_{on}} & \frac{1}{L_o+3L_{on}} \\ \frac{1}{C} & -\frac{1}{C} & 0 \end{bmatrix},$$

$$\mathbf{G}_\gamma = \frac{\omega_B}{L+3L_n} [1\ 0\ 0]^\top, \quad \mathbf{M}_\gamma = -\frac{\omega_B}{L_o+3L_{on}} [0\ 1\ 0]^\top,$$

that define the continuous-time model

$$\dot{\mathbf{x}}_\gamma(t) = \mathbf{F}_\gamma \mathbf{x}_\gamma(t) + \mathbf{G}_\gamma u_\gamma(t) + \mathbf{M}_\gamma w_\gamma(t). \quad (5)$$

Notice that (5) is independent of (1). By discretizing the system in the same way as (3), it results in

$$\mathbf{x}_\gamma(k+1) = \mathbf{A}_\gamma \mathbf{x}_\gamma(k) + \mathbf{B}_\gamma u_\gamma(k) + \mathbf{T}_\gamma w_\gamma(k). \quad (6)$$

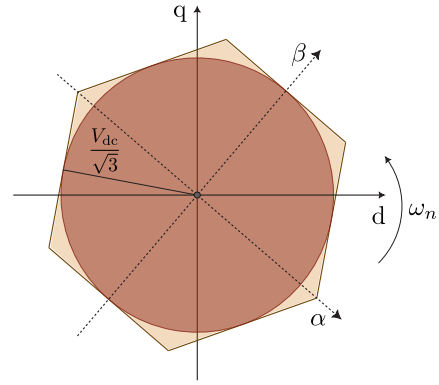


Fig. 3: The dq feasible set (hexagon) and its approximation (inscribed circle).

III. MODEL PREDICTIVE CONTROL PROBLEM

The system is controlled by solving an optimization problem in real time, at each instant k , every T_s second. The states of the system are sampled at each time step, with $\mathbf{x}(k) = \mathbf{x}_0$ and $x_\gamma(k) = x_{\gamma 0}$ being the sampled states. Similarly, $\mathbf{w}(k) = \mathbf{w}_0$ and $w_\gamma(k) = w_{\gamma 0}$ are the sampled disturbances. The MPC problem considers a prediction horizon of N steps and uses a receding horizon policy. The main objective of the strategy is for the converter and the filter to behave as a balanced voltage source behind impedance (i.e., \mathbf{v}_c must be balanced in steady state and change as slowly as possible, which is equivalent to $\mathbf{v}_{c,dq}$ being as constant as possible and $v_{c,\gamma} = 0$). Moreover, during balanced conditions (normal operation), it must properly track active and reactive power references. These objectives should be met while limiting the amplitude of the converter's current and the filter capacitor voltage for safety reasons.

A. Cost function

The cost function of the MPC problem must consider all objectives. Therefore, for the dq variables, the same objectives as in the three-wire case are proposed [1]:

$$J_{dq} = J_v + J_u + J_y, \quad (7)$$

comprising the following three terms:

$$\begin{aligned} J_v &= \lambda^v \sum_{\ell=k+1}^{k+N} \|\delta_{v_c}(\ell)\|^2, \quad J_u = \lambda^u \sum_{\ell=k}^{k+N-1} \|\delta_u(\ell)\|^2, \\ J_y &= \sum_{\ell=k+1}^{k+N} \|\mathbf{y}^*(\ell) - \mathbf{y}(\ell)\|_{\lambda^y}^2, \end{aligned} \quad (8)$$

where $\delta_{v_c}(\ell) = \mathbf{v}_{c,dq}(\ell) - \mathbf{v}_{c,dq}(\ell-1)$ and $\delta_u(\ell) = \mathbf{v}_{dq}(\ell) - \mathbf{v}_{dq}(\ell-1)$, while $\lambda^y = \text{diag}\{\lambda^p, \lambda^q\}$, and the \mathbf{K} -weighted norm is defined as $\|\xi\|_{\mathbf{K}} := \sqrt{\xi^\top \mathbf{K} \xi}$, with \mathbf{K} being a positive definite matrix. On the other hand, λ^p , λ^q , λ^v , and λ^u are weighting factors, tuned to define the priorities among the objectives. The term J_v penalizes the rate of change of $\mathbf{v}_{c,dq}$, to keep it as constant as possible. This leads to a balanced internal voltage (\mathbf{v}_c) behind impedance in steady state. On the other hand, the term J_u is added to regulate the aggressiveness and speed of the control loop with respect to

the dq variables. Lastly, J_y penalizes both active and reactive power tracking errors to address reference tracking during normal operation.

In relation to the γ variables, balanced capacitor voltages require $v_{c,\gamma}$ to be zero. For common-mode actuation, its amplitude must be penalized to regulate the aggressiveness of the γ control loop. Thus, the following terms are included in the cost function:

$$J_{v\gamma} = \lambda^{v\gamma} \sum_{\ell=k+1}^{k+N} \|v_{c,\gamma}(\ell)\|^2, \quad J_{u\gamma} = \lambda^{u\gamma} \sum_{\ell=k+1}^{k+N} \|v_\gamma(\ell)\|^2. \quad (9)$$

Due to the decoupling between the dq and the γ dynamics, as well as the decoupled objectives, the formulation so far appears as a trivial extension of the approach proposed in [1]. However, as will be shown in the next section, the dynamics are coupled through the constraints of the problem, increasing the complexity of both the system dynamic behavior and the control design challenge.

B. Constraints

This strategy allows to directly bound the system states, enhancing the safety of the converter and the system. To this end, the following constraints are defined.

1) *Converter voltage constraint*: The output voltages that a VSC can generate are defined by the topology used. For a four-legs two-level converter, the voltages the converter can generate in the $\alpha\beta\gamma$ frame are shown in Fig. 2. Recall that the dq frame is equivalent to the $\alpha\beta$ frame but rotates around the γ axis, as shown in Fig. 3. Regarding the feasible dq voltage components, since in the $\alpha\beta$ frame the feasible set corresponds to a hexagon, in the dq frame it rotates at an angular frequency ω_n , as depicted in Fig. 3. The set of voltages the converter can generate is, in simple terms, the extrusion of the hexagon along the γ axis in both positive and negative directions. This extrusion continues until $v_\gamma = \pm V_{dc}/3$, where the hexagon begins to shrink, until it reaches the points $v_\gamma = \pm V_{dc}$, where $\mathbf{v}_{dq} = [0, 0]^T$. In this work, for simplicity, the hexagon is approximated by its inscribed circle of radius $V_{dc}/\sqrt{3}$ (see Fig. 3). Therefore,

$$\mathbf{v}_{dq}^\top \mathbf{v}_{dq} \leq \left(\frac{V_{dc}}{\sqrt{3}} \right)^2 \quad (10)$$

The γ component, for simplicity, is constrained as

$$-\frac{V_{dc}}{3} \leq v_\gamma \leq \frac{V_{dc}}{3}, \quad (11)$$

which is a restrictive approximation of the original set and results in a cylinder inside the reachable voltages of the converter, as shown in Fig. 2.

2) *Converter current limitation*: Power electronic devices have limited overcurrent and overvoltage capabilities. Therefore, large currents can cause damage to the converter or trigger protection mechanisms that disconnect the converter and cut off the service provided. Hence, it is important to limit the currents to remain below the maximum value they can safely conduct. Such a constraint can be written as

$$i_d^2 + i_q^2 + i_\gamma^2 \leq I_{\max}^2. \quad (12)$$

which is an approximation of the box constraint that results from directly imposing constraints on the converter currents such as

$$-I_{\max} \leq i_x \leq I_{\max}, \quad \forall x \in \{a, b, c\}.$$

3) *Capacitor voltage constraint*: Grid codes generally define a voltage range considered normal operation, e.g., 0.9–1.1 p.u. [9]. Additionally, since overvoltages can damage the converter and increase the filter capacitor failure in time, limiting the filter capacitor voltage improves safety. Therefore, to protect the converter and the filter from overvoltages, the following constraint is added:

$$v_{c,d}^2 + v_{c,q}^2 + v_{c,\gamma}^2 \leq V_{\max}^2, \quad (13)$$

which is the same type of approximation as the one done for the converter current.

C. MPC problem formulation

The resulting MPC problem that is solved at each control instant k is

$$\min J_y + J_v + J_u + J_{v\gamma} + J_{u\gamma} \quad (14a)$$

s.t.

$$\begin{aligned} \mathbf{x}(\ell+1) &= \mathbf{A}\mathbf{x}(\ell) + \mathbf{B}\mathbf{u}(\ell) + \mathbf{T}\mathbf{w}(\ell), \\ \mathbf{x}_\gamma(\ell+1) &= \mathbf{A}_\gamma \mathbf{x}_\gamma(\ell) + \mathbf{B}_\gamma u_\gamma(\ell) + \mathbf{T}_\gamma w_\gamma(\ell), \end{aligned} \quad (14b)$$

$$\forall \ell \in \mathcal{K}_{0:N-1}$$

$$\mathbf{y}(\ell) = \mathbf{f}(\mathbf{x}(\ell)), \quad \forall \ell \in \mathcal{K}_{1:N} \quad (14c)$$

$$\mathbf{x}(k) = \mathbf{x}_0, \quad \mathbf{x}_\gamma(k) = \mathbf{x}_{\gamma,0} \quad (14d)$$

$$\mathbf{w}(\ell) = \hat{\mathbf{w}}(\ell), \quad \mathbf{w}_\gamma(\ell) = \hat{\mathbf{w}}_\gamma(\ell), \quad \forall \ell \in \mathcal{K}_{0:N-1} \quad (14e)$$

$$i_d^2(\ell) + i_q^2(\ell) + i_\gamma^2(\ell) \leq I_{\max}^2, \quad \forall \ell \in \mathcal{K}_{1:N} \quad (14f)$$

$$v_{c,d}^2(\ell) + v_{c,q}^2(\ell) + v_{c,\gamma}^2(\ell) \leq V_{\max}^2, \quad \forall \ell \in \mathcal{K}_{1:N} \quad (14g)$$

$$\mathbf{v}_{dq}^\top(\ell) \mathbf{v}_{dq}(\ell) \leq \left(\frac{V_{dc}}{\sqrt{3}} \right)^2, \quad \forall \ell \in \mathcal{K}_{0:N-1}, \quad (14h)$$

$$-\frac{V_{dc}}{3} \leq v_\gamma(\ell) \leq \frac{V_{dc}}{3}, \quad \forall \ell \in \mathcal{K}_{0:N-1}. \quad (14i)$$

where (14b) and (14c) are the system's state-space equations, used to predict the states and outputs along the prediction horizon, (14d) is the measurement of the states, used as the initial condition for the prediction, (14e) introduces the estimation $\hat{\mathbf{w}}$ of the disturbance along the prediction horizon, (14f) and (14g) are the limitations of the system states, and (14h) with (14i) define the feasible control set. The steps in the prediction horizon are defined by the ordered set $\mathcal{K}_{\eta:\xi} = \{k + \eta, \dots, k + \xi\}$, comprising consecutive instants starting from $k + \eta$, with $\eta < \xi$.

Notice how the dq dynamics are completely decoupled from the γ dynamics. However, the constraints (14f), (14g), (14h), and (14i) couple the behaviors and force the decision-making process to consider all components simultaneously to provide safe operation.

IV. SIMULATION RESULTS

The strategy was tested through the simulation of the system in Fig. 1 using the average model of the converter and the parameters in Table I, which are the same as [11],

TABLE I: System parameters for simulation

Parameter	Value	Parameter	Value
S_{nom}	20 kVA	V_{nom}	220 V (RMS, L-N)
V_{dc}	800 V	L_g	0.1731 pu
R	0.138 pu	R_o	0.0344 pu
L	0.1082 pu	L_o	0.0865 pu
C	0.2281 pu	R_g	0.0344 pu
R_n	0 pu	L_n	0 pu
R_{on}	0 pu	L_{on}	0 pu

but with a larger total impedance on the grid side, with the purpose of making the grid weaker, resulting in a more challenging setup. The worst-case scenario is analyzed, so the neutral wire is ideal (resistances and inductances are zero); therefore, the common-mode dynamics have smaller damping and impedance in the circulation path (see F_γ). The optimization problem was solved using `acados` [12], an open-source package of fast solvers for nonlinear optimization. A prediction horizon of $N = 50$ was used to explore the best possible performance. The sampling frequency was set at 10 kHz. The strategy is not tested in normal balanced-grid scenarios since it yields the same performance as in [1].

The weighting factors were set to prioritize balanced voltages at the filter capacitor, aiming for the converter and the filter to behave as a balanced voltage source behind impedance from the grid's perspective. During faults, emergency weighting factors are allowed to modify the priorities of control objectives, as will be explained for each case. The system was tested under the assumption that disturbances cannot be predicted, so they are kept constant throughout the horizon and equal to the measured disturbance w_0 at instant k (i.e., $\hat{w}(\ell) = w_0, \forall \ell \in \mathcal{K}_{0:N-1}$). This is done even though $v_{o,dq}$ can actually change over time, leading to errors in predicted behavior whenever the system is not in a perfectly balanced steady state (which is equivalent to a constant $v_{o,dq}$). A bigger priority is given to keeping v_c balanced and making the controller actuation less aggressive, so the weights in the cost function are set as $\lambda^p = \lambda^q = 1$, and $\lambda^v = \lambda^u = 10$ during normal operation. For common-mode terms $\lambda^{v\gamma} = \lambda^{u\gamma} = 10$. The first scenario tested was a symmetric voltage dip to evaluate the performance during a large, balanced grid disturbance, and to verify that the strategy does not inject common-mode when it is not needed. The second scenario is a two-phase dip, where the grid voltage includes positive, negative, and zero sequence components. In this scenario, the main task is to verify that all control objectives are met without violating the constraints on the states and actuation. In both cases $I_{\text{max}} = 1.5$ pu and $V_{\text{max}} = 1.1$ pu.

A. Symmetric voltage dip

While the converter operates at nominal active power, a symmetric voltage dip to 0.1 pu is applied to $v_{g,abc}$. Since during faults the tracking of power references is not relevant, λ_p and λ_q have to be small. Hence, λ_q is set to zero, while λ_p is left unchanged. On the other hand, to avoid an aggressive response, λ^u is set as $\lambda^u = 100$. The main objective of this test is to verify that the same performance of the three-wire

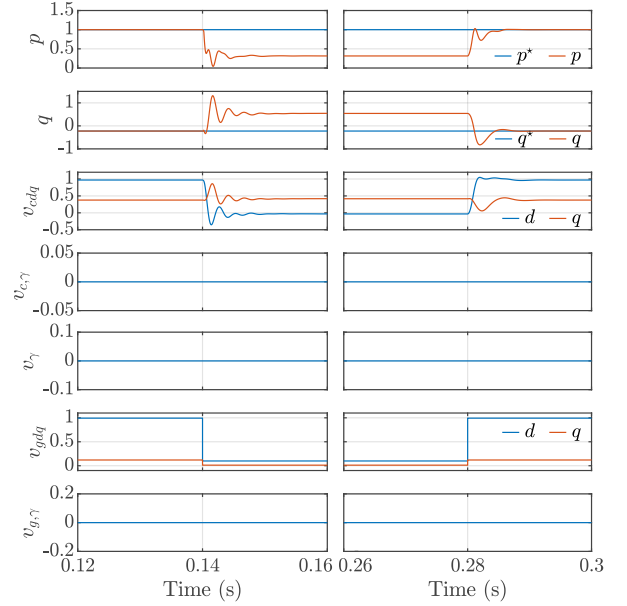


Fig. 4: Traces after inception and recovery from a 3-phase dip.

system is maintained; which means that the control strategy does not inject an unnecessary common-mode component.

As seen in Fig. 4, the controller responds quickly to the fault, reducing the capacitor voltage and injecting the maximum current, as required by the grid codes to activate protection mechanisms downstream. Notice that the capacitor voltage rapidly reaches a balanced steady state, with the controller injecting zero common-mode, as expected. Regarding the satisfaction of constraints, 5 shows that the converter current reaches its limit, as desired, while all other constraints are properly respected after both the inception and the clearance of the fault.

B. Asymmetric voltage dip

This experiment tests the capability of the control strategy to maintain the balanced voltage source behind impedance behavior of the converter during unbalanced conditions, including common-mode disturbance, in a four-wire system. With the system in nominal operation, two phases of $v_{g,abc}$ drop to 0.4 pu, while the third stays at 1 pu. In this case the most relevant objective is to keep v_c balanced, so the weighting factors are set as $\lambda^q = 0$, $\lambda^p = 10^{-3}$, λ^u is kept constant, while $\lambda^v = 10^5$ during the dip. Regarding the γ components, a high priority is given to removing the common-mode component of v_c to achieve balanced voltages; thus, $\lambda^{v\gamma}$ is set to $\lambda^{v\gamma} = 10^5$, while $\lambda^{u\gamma}$ remains constant.

The resulting behavior is shown in Fig. 6, where the following key points can be observed. First, the dq components of v_c remain constant despite the negative sequence introduced by the grid, demonstrating how the control strategy compensates for it, even with the incorporation of the common-mode components into the problem. Second, the γ component of the capacitor voltage is forced to zero by the

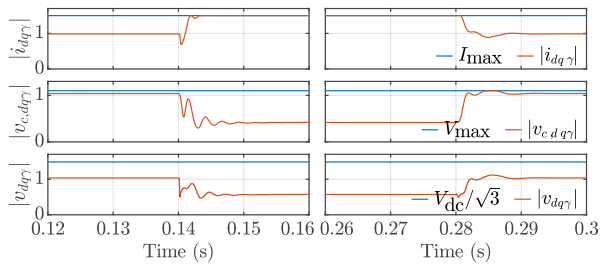


Fig. 5: Constraints after inception and recovery from a 3-phase dip.

injection of the converter voltage common-mode. As a result, the capacitor voltages are perfectly balanced, presenting only positive sequence and achieving the desired behavior of a balanced voltage source behind an impedance. Finally, as shown in Fig. 7, all the constraints imposed by the controller on the states and the actuation are satisfied. These results show the effectiveness of the proposed strategy in achieving all control objectives simultaneously.

V. CONCLUSION AND FUTURE WORK

The manuscript presents the control problem of a converter connected to four-wire LV networks. To solve it, a nonlinear MPC strategy was proposed. This strategy allows imposing direct constraints on the system's states while controlling the power injected into the grid and yielding a balanced voltage source behind impedance behavior. The strategy was tested with symmetric and asymmetric faults, showing the controller's ability not only to control the dq variables of the system, but also to deal with the common mode injected by the grid. This resulted in constraint satisfaction while meeting all control objectives simultaneously. Even though the results are promising, extensive testing of the strategy is necessary to validate its effectiveness against a variety of types and depths of faults, with different levels of grid strengths and filter parameters. Moreover, the real-time viability of the strategy must also be addressed since solving the proposed MPC problem is computationally demanding. Finally, a systemic analysis is needed to validate the positive impact of this strategy on power systems with IBRs operated by it.

REFERENCES

- [1] C. González, L. Costa, and G. Papafiotou, "Universal constrained power flow control for grid-tied power electronics converters," in *2025 European Control Conference (ECC)*, June 2025.
- [2] D. Dong, B. Wen, D. Boroyevich, P. Mattavelli, and Y. Xue, "Analysis of phase-locked loop low-frequency stability in three-phase grid-connected power converters considering impedance interactions," *IEEE Transactions on Industrial Electronics*, vol. 62, no. 1, pp. 310–321, Jan 2015.
- [3] X. Gao, D. Zhou, A. Anvari-Moghaddam, and F. Blaabjerg, "Stability analysis of grid-following and grid-forming converters based on state-space modelling," *IEEE Transactions on Industry Applications*, vol. 60, no. 3, pp. 4910–4920, May 2024.
- [4] M. Wang, K. Meng, L. Yu, L. Yuan, and Z. Liang, "Comparative fault ride through assessment between grid-following and grid-forming control for weak grids integration," in *2022 IEEE Global Conference on Computing, Power and Communication Technologies (GlobConPT)*, Sep. 2022, pp. 1–6.

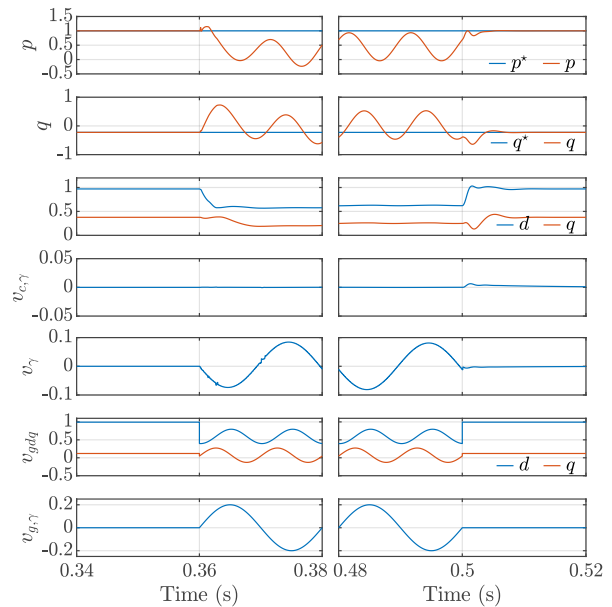


Fig. 6: Traces after inception and recovery from a 2-phase dip.

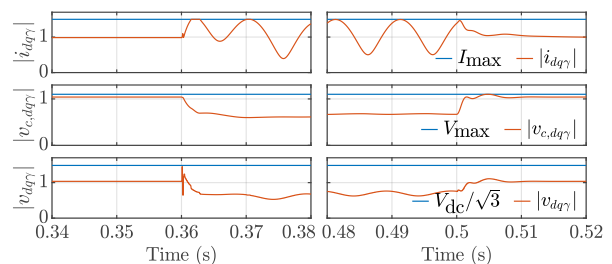


Fig. 7: Constraints after inception and recovery from a 2-phase dip.

- [5] J. Jia, G. Yang, and A. H. Nielsen, "A review on grid-connected converter control for short-circuit power provision under grid unbalanced faults," *IEEE Transactions on Power Delivery*, vol. 33, no. 2, pp. 649–661, April 2018.
- [6] N. Baeckeland, D. Chatterjee, M. Lu, B. Johnson, and G.-S. Seo, "Overcurrent limiting in grid-forming inverters: A comprehensive review and discussion," *IEEE Transactions on Power Electronics*, vol. 39, no. 11, pp. 14 493–14 517, Nov 2024.
- [7] S. F. Zarei, H. Mokhtari, M. A. Ghasemi, and F. Blaabjerg, "Reinforcing fault ride through capability of grid forming voltage source converters using an enhanced voltage control scheme," *IEEE Transactions on Power Delivery*, vol. 34, no. 5, pp. 1827–1842, Oct 2019.
- [8] M. Shirazi, D. Gross, D. Light, J. VanderMeer, and T. Morgan, "Evaluation of current-limiting strategies for grid-forming inverters," in *2023 IEEE Energy Conversion Congress and Exposition (ECCE)*, Oct 2023, pp. 1067–1074.
- [9] National Energy System Operator, "The complete grid code. Issue 6, Revision 27, 01 October 2024. [Online] Available: <https://dcm.nationalenergyso.com/> (Revisited: October 7th, 2024)."
- [10] T. Geyer, *Model Predictive Control of High Power Converters and Industrial Drives*. Wiley, 2016.
- [11] S. Jiang, Y. Zhu, T. Xu, and G. Konstantinou, "Current-synchronization control of grid-forming converters for fault current limiting and enhanced synchronization stability," *IEEE Transactions on Power Electronics*, vol. 39, no. 5, pp. 5271–5285, May 2024.
- [12] R. Verschuere, G. Frison, D. Kouzoupis, J. Frey, N. van Duijkeren, A. Zanelli, B. Novoselnik, T. Albin, R. Quirynen, and M. Diehl, "acados – a modular open-source framework for fast embedded optimal control," *Mathematical Programming Computation*, 2021.